Food Chemistry: X 23 (2024) 101618

Contents lists available at ScienceDirect

Food Chemistry: X

journal homepage: www.sciencedirect.com/journal/food-chemistry-x

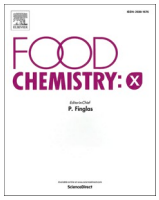

Sensitive and specific detection of *Listeria monocytogenes* in food samples using imprinted upconversion fluorescence probe prepared by emulsion polymerization method

Taotao Ren [a,b,1], Yiwei Lu [a,1], Peng Liu [a], Xuelian Hu [a], Wenxiu Wang [a], Shuo Wang [c,a], Xiuying Liu [d,*], Yiwei Tang [a,*]

[a] College of Food Science and Technology, Hebei Agricultural University, Baoding 071001, China
[b] College of Food Science & Project Engineering, Bohai University, Jinzhou 121013, China
[c] Tianjin Key Laboratory of Food Science and Health, School of Medicine, Nankai University, Tianjin 300071, PR China
[d] School of Food Science and Engineering, Wuhan Polytechnic University, Wuhan 430028, China

ARTICLE INFO

Keywords:
Upconversion fluorescence
Bacteria imprinting
Listeria monocytogenes
Pickering emulsion polymerization
Salmon
Chicken breast

ABSTRACT

Listeria monocytogenes (*L. monocytogenes*) is a foodborne pathogen with high morbidity and mortality rates, necessitating rapid detection methods. Current techniques, while reliable, are labor-intensive and not amenable to on-site testing. We report the design and synthesis of a novel imprinted upconversion fluorescence probe through Pickering emulsion polymerization for the specific detection of L. *monocytogenes*. The probe employs trimethylolpropane trimethacrylate and divinylbenzene as cross-linkers, acryloyl-modified chitosan as a functional monomer, and the bacterium itself as the template. The developed probe demonstrated high specificity and sensitivity in detecting L. *monocytogenes*, with a limit of detection of 72 CFU/mL. It effectively identified the pathogen in contaminated salmon and chicken samples, with minimal background interference. The integration of molecular imprinting and upconversion fluorescence materials presents a potent and reliable approach for the rapid and specific detection of L. *monocytogenes*, offering considerable potential for on-site food safety testing.

1. Introduction

Listeria monocytogenes (L. monocytogenes), a Gram-positive, non-spore-forming rod-shape bacterium, stands out as a notable foodborne pathogen with a considerable mortality rate (20%–40%), leading to listeriosis-an alarming health threat to animals and humans (Liu et al., 2023; Myndrul et al., 2024). Owing to its extraordinary resilience in a variety of environmental conditions, including a broad pH spectrum (4.3 to 9.4), high salt concentrations, and low temperatures, this bacterium has been detected in an array of foods, as well as in water and soil (Prasad et al., 2024; Zakrzewski, Gajewska, Chajęcka-Wierzchowska, Załuski, & Zadernowska, 2023). Staggeringly, 99% of listeriosis outbreaks were traceable to food products harboring this pathogen (Duze, Marimani, & Patel, 2021). Therefore, there is an imperative and urgent call for the development of innovative, expeditious, and trustworthy methods for the detection of L. *monocytogenes*.

While traditional culture and biochemical analysis-based microbiological identification techniques are well-established for L. *monocytogenes* detection, their resource-intensive and protracted nature constrains their utility for on-site and rapid testing (Li et al., 2021; Magalhães et al., 2021).To mitigate the limitations of these conventional approaches, molecular biology strategies (e.g., polymerase chain reaction, nucleic acid molecule hybridization, and loop-mediated isothermal amplification) have been employed for identifying this foodborne pathogen (Bundidamorn, Supawasit, & Trevanich, 2021; Ren et al., 2024; Roumani, Azinheiro, Carvalho, Prado, & Garrido-Maestu, 2021). Nevertheless, these techniques often necessitate expertise, sophisticated equipment, costly materials, and/or intricate protocols (Liu et al., 2021). Moreover, antibody-based immunochromatographic point of care test (Lopes-Luz et al., 2023), fluorescence assays (Li et al., 2022), and lateral flow immunoassays (Tominaga, 2017) provide alternatives for detecting L. *monocytogenes*. Despite expediting the analytical process, these immunological methods may generate considerable waste due to the extensive use of samples and reagents (Silva, Neves, Magalhães, Freire,

* Corresponding author.
E-mail address: tangyiwei81@163.com (Y. Tang).
[1] These authors contributed to the work equally and should be regarded as co-first authors.

https://doi.org/10.1016/j.fochx.2024.101618
Received 1 February 2024; Received in revised form 10 June 2024; Accepted 2 July 2024
Available online 4 July 2024

& Delerue-Matos, 2020). Consequently, there is a continuing need to invent new sensing techniques that are straightforward, cost-effective, precise, and highly sensitive.

Recently, some novel materials-based approaches for removal or detecting hazardous substances have been drawing increased attention due to their simplicity, rapidness, low cost, solid stability, high selectivity, and/or sensitivity (Guk et al., 2024; Xiao, Al-Nayili & Alhaidry, 2023; Salman & Alshamsi, 2022; Xiao et al., 2023; Basak, Venkatram, & Singhal, 2022; Pan et al., 2022). Notably, biosensors integrated with molecularly imprinted polymers (MIPs) on various transducer platforms have emerged as highly sensitive and selective candidates for ultra-rapid bacterial detection (Zhang, Wang, & Lu, 2021). The molecular imprinting technique is a sophisticated strategy for creating synthetic receptors, termed molecularly imprinted polymers (MIPs), which exhibit high specificity and selectivity toward their respective targets (Liu et al., 2024). Employed as recognition elements, MIPs have gained widespread application in electrochemical sensors, fluorescence probes, and adsorption materials, boasting the ability to bind targets rapidly and specifically, affordability, and precise detection capabilities for various applications including monitoring chemical pollutants, cancer treatment, sample processing, and chromatographic separation (Cardoso, Martins, Lanças, & Chaves, 2023; Chen et al., 2024). Recent advances have seen MIPs integrated into biosensors for highly sensitive and selective bacterial detection, marking a notable expansion in their application (Dar, Shao, Tan, & Lv, 2020; Jamieson et al., 2021).

A fluorescent nanohybrid quantum dots complex, as reported by Donoso et al., facilitates the swift observation of L. *monocytogenes* at a concentration of 5.19×10^3 CFU/mL utilizing epifluorescence microscopy (Donoso et al., 2017). A visual detection technique, developed by Zhao et al., achieves a limit of detection for L. *monocytogenes* of 10^3 CFU/mL by incorporating fluorescent molecularly imprinted polymers with CdTe quantum dots (Zhao, Cui, Wang, & Wang, 2019). While these quantum dot-based methods provide a strong candidate for detecting L. *monocytogenes*, they yield semi-quantitative results and are hampered by drawbacks such as intrinsic toxicity and considerable autofluorescence interference (Guan et al., 2023). In contrast, rare-earth doped upconversion fluorescence materials (UFMs) are distinguished by their relatively low toxicity, superior photochemical stability, almost nonexistent background interference, consistent emission, large Stokes shifts, and deep penetration into biological samples, earning recognition as an excellent fluorescent label (Aleem et al., 2024; Liu, Liu, et al., 2023). Attributable to their unique anti-Stokes fluorescence properties-absorbing near-infrared and converting it to visible light-UFMs possess outstanding optical properties and are considered highly promising for the accurate and sensitive detection of L. *monocytogenes*. Despite these advantages, the integration of MIPs with UFMs for the sensing of pathogenic bacteria is an area that remains underexplored.

In this study, our objective was to engineer a molecularly imprinted upconversion fluorescence probe that offers both sensitivity and specificity for the detection of L. *monocytogenes*. The fabrication of MIPs-based probe was first accomplished through Pickering emulsion polymerization, employing trimethylolpropane trimethacrylate and divinylbenzene as the cross-linking agents, *L. monocytogenes* as the template organism, and acryloyl-modified chitosan as the functional monomer. Characterized as an innovative upconversion fluorescence probe, it has been applied to detect L. *monocytogenes* in both salmon and chicken sample matrices. It is hypothesized that the novel probe will exhibit enhanced performance in the detection of L. *monocytogenes*, characterized by high precision and negligible background interference, thus representing a substantial advancement over current detection methodologies.

2. Material and methods

2.1. Materials

Yttrium chloride hexahydrate ($YCl_3 \cdot 6H_2O$, 99%), ytterbium chloride hexahydrate ($YbCl_3 \cdot 6H_2O$, 99%), erbium chloride hexahydrate ($ErCl_3 \cdot 6H_2O$, 99%), sodium hydroxide (NaOH, 99%), oleic acid, 1-octadecene, diethylene glycol, polyacrylic acid (M.W.: ~2000 D), trimethylolpropane trimethacrylate (TRIM), divinylbenzene (DVB), dibenzoyl peroxide (BPO), acryloyl chloride, N. *N*-dimethylaniline (DMA), 1-(3-dimethylaminopropyl)-3-ethylcarbodiimide hydrochloride (EDC), N-hydroxysuccinimide (NHS) and sodium dodecyl sulfate (SDS) were sourced from Aladdin (Shanghai, China, https://www.aladdin-e.com/). Chitosan (M.W.: 50,000–190,000 D) was acquired from Sigma-Aldrich (Shanghai, China, https://www.sigmaaldrich.cn/). Brain heart infusion (BHI) for culturing L. *monocytogenes* was obtained from Hopebiol Biotechnology Co., Ltd. (Qingdao, China, https://www.hopebiol.com/). All other reagents were procured from Sinopharm Chemical Reagent Co., Ltd. (Shanghai, China, https://en.reagent.com.cn/) and Tianjin Chemical Reagent Factory (Tianjin, China, https://guide18159.guidechem.com/).

2.2. Apparatus and characterizations

The morphology and elemental composition of the prepared samples were characterized using a Hitachi S-4800 (Japan) scanning electron microscope (SEM) that is paired with X-ray energy dispersive spectroscopy (Hitachi S-4800, Japan). Fourier transform infrared (FT-IR) spectra of the characteristic groups were captured by a Vector 22 Fourier transform infrared spectrometer (Bruker, German) employing the KBr disc method in a range of 4000–400 cm^{-1}. The crystalline structures present in the samples were analyzed via X-ray diffraction (XRD) patterns obtained by a UItima IV X-ray power diffractometer equipped with a Cu Kα radiation source (Rigaku Corporation, Japan). A Pyris Diamond TG/DTA analyzer (Perkin Elmer, Japan) was used for thermogravimetric analyses of samples with a heating rate of 10 °C/min in nitrogen. Fluorescence spectra were obtained on a Hitachi F-7000 spectrophotometer (Japan) complemented by an external 0–5 W adjustable 980 nm semiconductor laser (Changchun Leishi Optoelectronic Co., China).

2.3. Synthesis of β-$NaYF_4$: Yb^{3+}, Er^{3+} upconversion nanoparticles

The β-$NaYF_4$: Yb^{3+}, Er^{3+} upconversion nanoparticles (UCNPs) were synthesized by the high-temperature pyrolysis method according to the reported method with slight modifications [34]. Specifically, $YCl_3 \cdot 6H_2O$ (0.243 g), $YbCl_3 \cdot 6H_2O$ (0.0698 g), and $ErCl_3 \cdot 6H_2O$ (0.0077 g) were added into a flask with three necks containing oleic acid (3.0 mL) and 1-octadecene (17.0 mL), and the mixture was stirred at 160 °C for 30 min under argon protection. After cooling to room temperature of the flask with three necks, 10 mL methanol solution containing 0.1 g sodium hydroxide and 0.148 g ammonium fluoride were gradually dropped into the reaction solution, and mixed by stirring for 30 min. Then, methanol was removed by evaporation, and the mixture was heated at 310 °C for 90 min under argon protection. After the reaction, the UCNPs were isolated by precipitation and centrifugation and then purified with a mixed solution of ethanol and cyclohexane (1:1; *v*/v) and finally dried in an oven at 60 °C.

2.4. Synthesis of polyacrylic acid-modified UCNP

Polyacrylic acid (0.75 g) and diethylene glycol (15 mL) in a flask were mixed at 110 °C for 60 min under argon protection. Subsequently, toluene (3 mL) containing UCNPs (45.0 mg) was added in the flask. The chemical reaction was carried out for 60 min at 240 °C under argon. After the flask was cooled to room temperature, the polyacrylic acid-

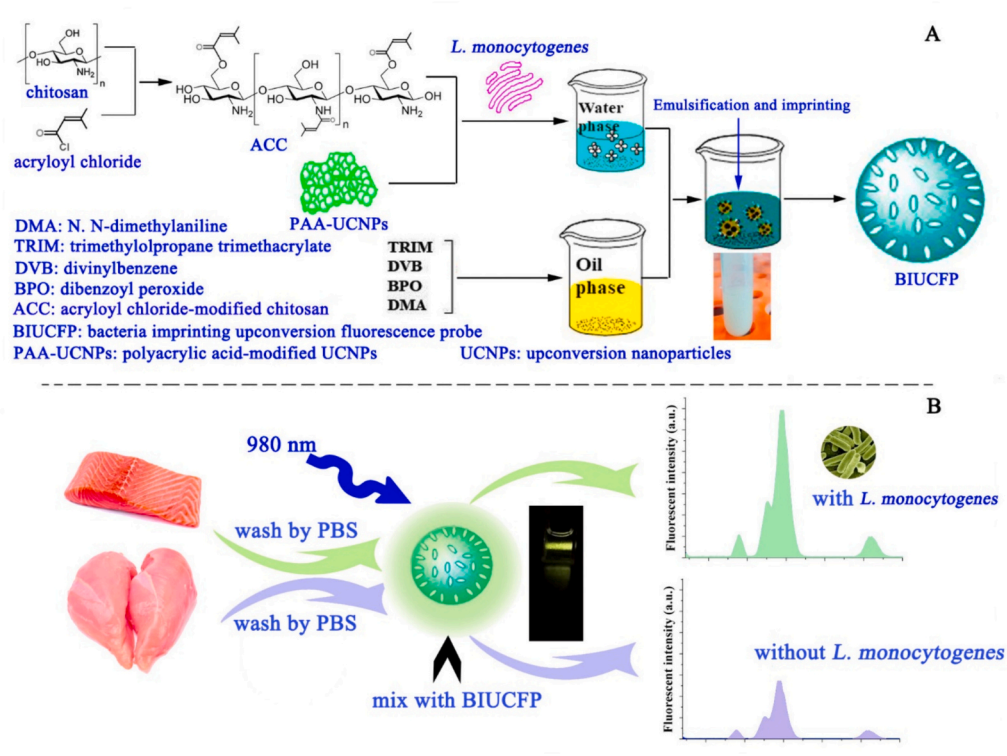

Scheme 1. Schematic illustration of the preparation process of the BIUCFP (A) and BIUCFP-based fluorescence analysis method (B).

modified UCNPs (PAA-UCNPs) were obtained by centrifugation (8157 ×*g* for 15 min) and washed with ultrapure water three times, followed by drying in an oven.

2.5. Preparation of acryloyl chloride-modified chitosan (ACC)

Chitosan (0.805 g) was homogenized in 20 mL N. *N*-dimethylacetamide in a flask with three necks with ultrasonic assistance. Twelve hours later, the flask was moved into an ice-water bath. After removal of the dissolved oxygen by blowing argon for 10 min at 0 °C, triethylamine (500 μL) was added into the mixture and mixed by stirring. Then oxygen-free N. *N*-dimethylacetamide (2.5 mL) containing acryloyl chloride (325.4 μL) was added dropwise under constant stirring. Four hours later, the mixture was normalized to room temperature and the reaction was carried out for 20 h keeping stirring. Lastly, the products were purified with N. *N*-dimethylacetamide, dichloromethane, and methanol, respectively, for at least 3 times, and finally dried in an oven.

2.6. Synthesis of ACC@PAA-UCNPs composites

The ACC@PAA-UCNPs composites were synthesized by coupling the amino groups of ACC with the carboxyl groups of the PAA-UCNPs by the active ester method. First, PAA-UCNPs (2.0 mg) dispersed in 2 mL of MES buffer (pH 6.0, 0.01 M) were activated with EDC (120.0 μL, 5 mg/mL) and NHS (60 μL, 5 mg/mL). Following two hours, the activated PPA-UCNP was obtained by centrifugation, and washed with ultrapure water for 3 times, and then re-suspended in 2 mL ultrapure water. Further, 5 mL acetic acid solution (0.03%) containing 1.5 mg ACC was added into the PAA-UCNPs suspension. After a 12 h dark incubation, the ACC@PAA-UCNPs product was collected by centrifugation and washed with ultrapure water for 3 times.

2.7. Preparation of bacteria

Bacterial strains of L. *monocytogenes* ATCC 19111 (National Local Joint Engineering Research Center for storage, processing, and safety control technology of fresh agricultural products, Bohai University, China) were cultivated in BHI overnight at 30 °C and 160 rpm. Bacterial concentrations were assessed by optical density (OD) at 595 nm using a UV–vis 2550 spectrometer (Shimadzu, Japan).

2.8. Preparation of bacteria imprinting upconversion fluorescence probe (BIUCFP)

A 300 μL aliquot of the L. *monocytogenes* suspension ($OD_{595} \approx 2.0$) was combined with 900 μL of phosphate buffered solution (PBS, pH 7.4, 0.01 M) containing ACC@PAA-UCNPs (2.25 mg). The mixture was agitated for 3 h for self-assembly between the bacteria and ACC@PAA-UCNPs as the stabilizer. After the addition of the oil phase consisting of TRIM (450 μL), DVB (450 μL), BPO (8.0 mg), and DMA (31 μL), the Pickering emulsion was obtained by shaking vigorously. Then the polymerization was carried out at room temperature for 28 h. The polymer microparticles (BIUCFP) were isolated by centrifugation, cleansed successively with 10% acetic acid, 1% SDS solution, ultrapure water, and methanol five times, and desiccated in a vacuum oven. The non-imprinted upconversion fluorescence probe (NIUCFP) was prepared using the same procedure but without the template L. *monocytogenes*.

2.9. Fluorescence analysis

10 mg of BIUCFP and different concentrations of L. *monocytogenes*, ranging from 1×10^1 to 1×10^7 CFU/mL, were incubated in centrifugal tubes at room temperature with shaking for 2 h. After removal of the unbound bacteria by washing with 1.0 mL PBS (pH 7.4, 0.01 M), the BIUCFP was re-suspended in 1 mL deionized water, followed by recording the fluorescence spectrum of each resuspension solution over the wavelength range upon the excitation at 980 nm.

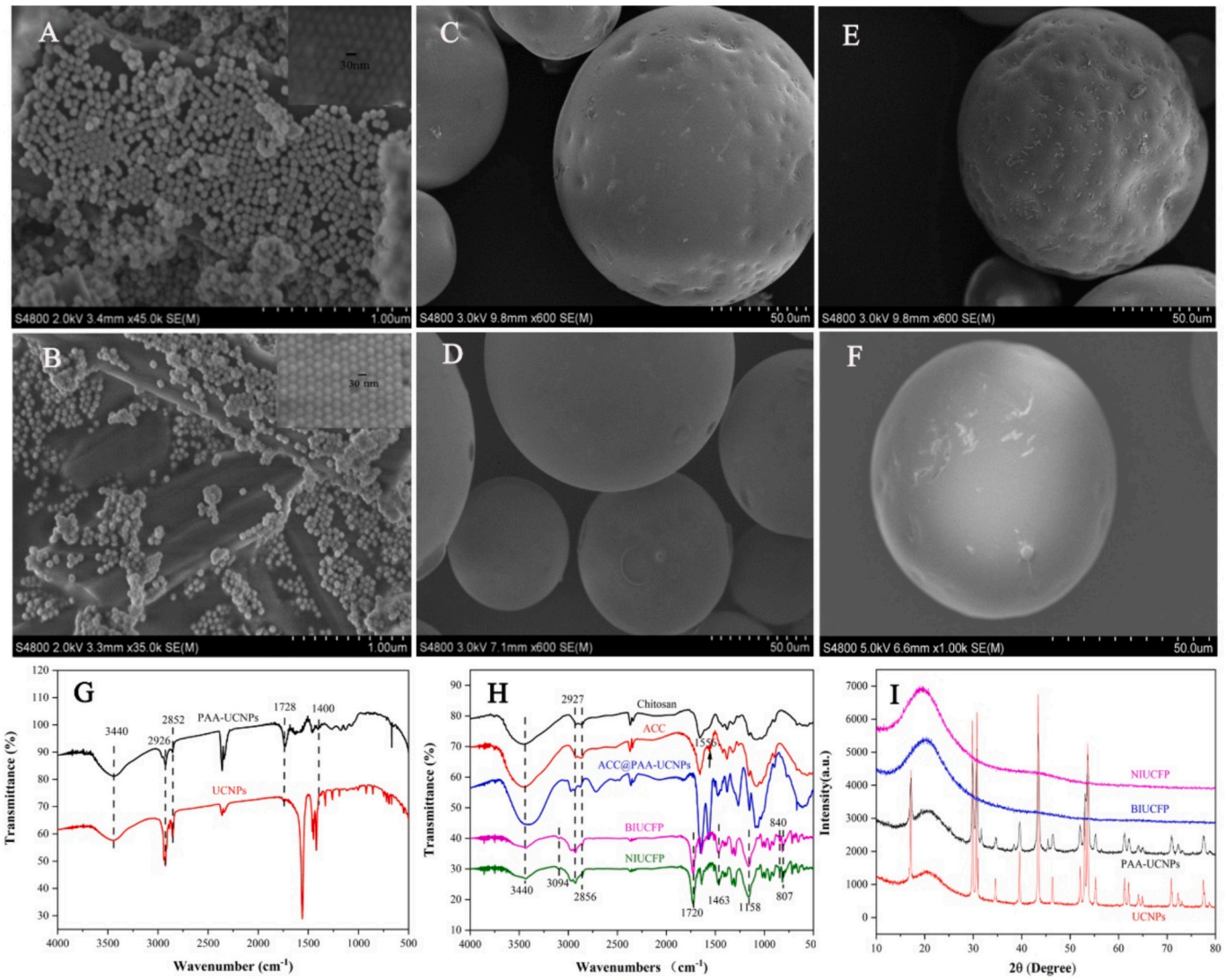

Fig. 1. Scanning electronic microscopy (SEM) image of UCNPs (A), PAA-UCNPs (B) , BIUCFP (C), NIUCFP (D), BIUCFP after adsorption of L. *monocytogenes* (E), and NIUCFP after adsorption of L. *monocytogenes* (F). FT-IR spectra of PAA-UCNPs and UCNPs (G). FT-IR spectra of Chitosan, ACC, ACC@PAA-UCNPs, BIUCFP and NIUCFP (H). XRD of UCNPs, PAA-UCNPs, BIUCFP, and NIUCFP (I).

2.10. Analysis of real sample

Salmon and chicken breast samples obtained from the local market were selected to evaluated the performance of the BIUCFP-based fluorescence analysis by spiking and recovery studies. First, the salmon and chicken breast were exposed to UV light for 30 min to obtain the L. *monocytogenes*-free samples. The samples were then cut into small pieces of equal mass in a clean workbench and placed in sterile sample bags. 17 mL of gradient diluted L. *monocytogenes* solution were added to each bag to completely immerse the meat pieces. The meat pieces were repeatedly kneaded and mixed, and refrigerated overnight at 4 °C. Then, the meat pieces were taken out and placed in another sterile sample bag. 17 mL of PBS was added to each bag to wash off the bacteria of the meat pieces, and the collected elution solution as the sample extract. The L. *monocytogenes* in the samples was determined by plating (Hammons, Stasiewicz, Roof, & Oliver, 2015) and the BIUCFP-based fluorescence analysis.

For salmon samples, the spiked levels were calculated to be the concentrations of 1.8×10^1 CFU/g, 4.0×10^1 CFU/g, 1.1×10^2 CFU/g, 1.9×10^3 CFU/g, 4.5×10^4 CFU/g, and 1.3×10^6 CFU/g. For chicken breast, the spiked levels were at the concentrations of 1.1×10^1 CFU/g, 5.5×10^1 CFU/g, 1.0×10^2 CFU/g, 2.2×10^3 CFU/g, 1.3×10^4 CFU/g, and 1.1×10^6 CFU/g.

3. Result and discussion

3.1. Synthesis of BIUCFP

The conformational integrity of the template cells during imprinting is crucial for selectivity of the imprinted polymer. To maintain integrity of the imprinting live bacteria, the BIUCFP was synthesized utilizing Pickering emulsion-based imprinting polymerization. Scheme 1 illustrates that chitosan is firstly modified with acryloyl chloride, introducing double bonds to *co*-polymerize with cross-linker. The functional chitosan is coupled with UCNPs by covalent bonds, avoiding the leakage problem of the nanoparticles during the application process. The self-assemblies are obtained by amalgamating the compound materials and L. *monocytogenes*, employed as the particle stabilizer to construct a stable emulsion of cross-linking monomers (the oil phase) in water (Cai et al., 2017). Oxidation-reduction reaction-driven radical polymerization takes place in the oil phase, and the self-assemblies are covalently fixed to the core of the polymer particles. After removing L. *monocytogenes* cell, the bacteria-imprinted sites are left on the surface of the particles.

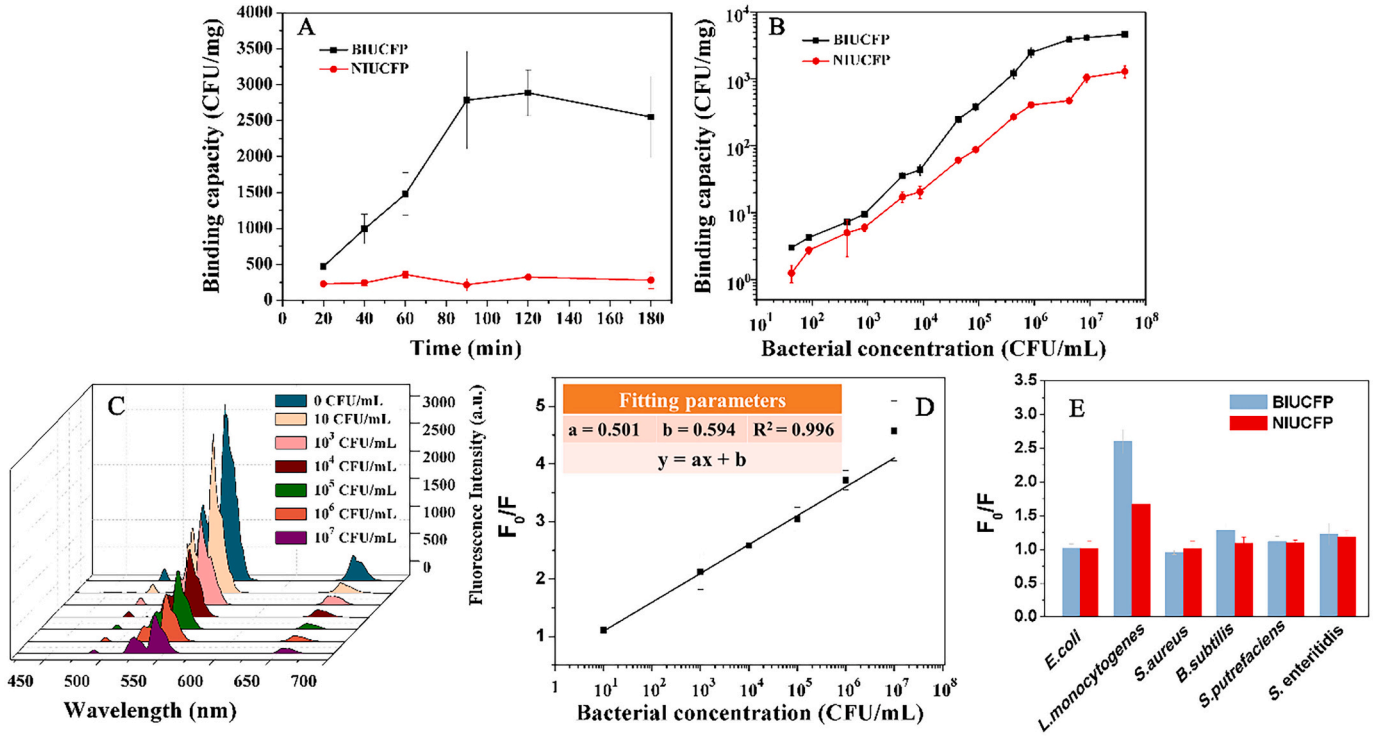

Fig. 2. Kinetic uptake plot of BIUCFP and NIUCFP (A) (BIUCFP or NIUCFP, 10 mg; *L. monocytogenes*, 1×10^5 CFU/mL). Adsorption isotherms of BIUCFP and NIUCFP (B) (BIUCFP or NIUCFP, 10 mg). Fluorescence spectra of BIUCFP (C) respond to varying concentrations of L. *monocytogenes* in the range from 1×10^1 to 1×10^7 CFU/mL and the corresponding calibration plot (D). Fluorescence response of BIUCFP to different species (E) (*L. monocytogenes*, 10^3 CFU/mL; other species, 10^5 CFU/mL).

3.2. Characterization

3.2.1. Morphological characterization

As shown in Fig. 1A, the morphological characteristics of UCNPs exhibited a hexagonal phase, characterized by uniform shape and an average diameter of approximately 30 nm. Compared to UCNPs, in Fig. 1B, the particles of PAA-UCNPs did not undergo significant changes in size. Nonetheless, following PAA modification, a more uniform distribution and a non-aggregated morphology were observed.

The PAA-UCNPs were subsequently processed with ACC to synthesize BIUCFP and the control group of NIUCFP, and the SEM results are also depicted in Fig. 1**.** As illustrated in Fig. 1C and Fig. 1D, both BIUCFP and NIUCFP exhibited a spherical shape. In comparison to the NIUCFP, the BIUCFP presented a rough morphology, featuring grooves on the surface of the particles. This phenomenon can be attributed to the presence of imprinted cavities originating from the template bacteria. In Fig. 1E and Fig. 1F, following exposure to the target bacteria, consistent adsorption of the target bacteria on the surface of BIUCFP was noted, attributable to their specific binding cavities. Moreover, a minor presence of bacteria was also detected on the surface of NIUCFP, suggesting non-specific adsorption.

3.2.2. EDS analysis

EDS analysis was conducted on the BIUCFP, with the findings illustrated in **Fig. S1**. The EDS characterization indicates that the BIUCFP particle contains elements including C, H, O, N, F, Yb, Y, and Er, further confirming the successful synthesis of polymers.

3.2.3. FT-IR analysis

The FT-IR spectroscopy analysis of UCNPs and PAA-UCNPs are illustrated in Fig. 1G. The absorption peaks at 2926 cm^{-1} and 2852 cm^{-1} corresponded to the stretching vibrations of methylene groups in the long chain of oleic acid ligands coating the surface of the UCNPs. Conversely, in the spectrum of PAA-UCNP, there was a pronounced reduction in the peaks at these two positions, indicating that the oleic acid ligands on the surface of UCNPs have been partially replaced. Furthermore, the peaks at 3440 cm^{-1}, 1728 cm^{-1}, and 1400 cm^{-1} were the stretching vibration of -OH, the vibrations of the C═O, and the bending vibration of O—H, respectively. The presence of these new peaks further corroborates the successful modification of UCNPs.

To ascertain the changes in functional groups pre- and post-preparation of the polymer, the FT-IR spectra of ACC@PAA-UCNPs, BIUCFP, and NIUCFP were examined. As depicted in Fig. 1H, the spectrum of ACC@PAA-UCNPs exhibited peaks at 1650 cm^{-1}, 3440 cm^{-1}, and 1560 cm^{-1}, which corresponded to the stretching vibration of the C═O group, the N—H bond, and the bending vibration of the N—H bond in the amide II band, respectively. These results indicated that the amino group on the ACC underwent a condensation reaction with the carboxyl group of PAA-UCNP, forming the ACC@PAA-UCNPs composite. As evidenced in Fig. 1H, in the spectrum of BIUCFP, the absence of the absorption peak at 1556 cm^{-1} implied that cross-linking reactions occur between the imprinting polymer and the double bond on ACC during the polymerization process. Moreover, the peaks at 1463 cm^{-1}, 1158 cm^{-1}, and 1720 cm^{-1}, denoted the bending vibration of the C—H group in the $-CH_3$ moiety, the stretching vibration of the C-O-C bond, and the C═O group, respectively, indicating the successful synthesis of BIUCFP. The similar absorption peak intensities of BIUCFP and NIUCFP revealed that the NIUCFP underwent a similar cross-linking polymerization reaction.

3.2.4. XRD analysis

In Fig. 1I, the XRD spectra of ACC@PAA-UCNPs, BIUCFP, and NIUCFP are presented. The peak positions of ACC@PAA-UCNPs indicated a pure-phase hexagonal crystal structure, aligning with existing literature (Mahata & Lee, 2019). However, within the diffraction spectra of both BIUCFP and NIUCFP, the diffraction peaks of ACC@PAA-UCNPs are less pronounced. This phenomenon likely results from the encapsulation by a dense, cross-linked polymer layer, which subsequently alters the diffraction patterns of the ACC@PAA-UCNPs.

3.3. Fluorescent property

To assess the impact of the bacteria template on the fluorescence characteristics of imprinted polymers, an analysis of BIUCFP's fluorescent properties was conducted both before and after template removal. As depicted in **Fig. S2**, in comparison to the BIUCFP retaining the template bacteria, the fluorescence intensity of the BIUCFP significantly increased after the removal of the template bacteria. This increase may be ascribed to the closer proximity and interactions between BIUCFP and template bacteria, leading to the fluorescent quenching of the UCNPs. Furthermore, the fluorescence intensity of NIUCFP was higher than that of BIUCFP containing the template. This phenomenon is likely due to the limited amount of residual template bacteria that could not be removed through the washing process in BIUCFP, leading to the quenching of the fluorescence of the UCNPs, and resulting in a lower fluorescent intensity.

3.4. Adsorption performance

3.4.1. Adsorption kinetics analysis

As illustrated in Fig. 2A, the adsorption capacity of BIUCFP demonstrates a rapid increase up to 90 min. Between 90 and 120 min of adsorption, the rate of increase in adsorption capacity begins to decelerate, eventually stabilizing at an equilibrium. Beyond 120 min, however, there is a noticeable decline in BIUCFP's adsorption capacity. This phenomenon may be attributed to the diminishing viability of the target bacteria over time, due to nutrient scarcity in the PBS buffer solution, potentially leading to apoptosis and consequently, a reduction in the adsorption capacity of BIUCFP. In contrast to BIUCFP, the control group NIUCFP showed consistently lower adsorption capacity for the target bacteria, with the adsorption trend remaining stable throughout the testing duration. The adsorption behavior of NIUCFP is primarily attributable to its physical adsorption mechanism. The adsorption capacities of BIUCFP and NIUCFP were 2886.7 CFU/mg and 323.3 CFU/mg, respectively.

The Pseudo-first-order (Eq. (1)), Pesudo-second-order (Eq. (2)), and Elovich (Eq. (3)) model,

$$ln(Q_e - Q_t) = lnQ_e - \frac{k_1 t}{2.303} \quad (1)$$

$$t/Q_t = 1/k_2 Q_e^2 + t/Q_e \quad (2)$$

$$Q_t = \frac{1}{\beta} ln(\alpha\beta) + \frac{1}{\beta} ln(t) \quad (3)$$

where Q_t (CFU/mg) and Q_e (CFU/mg) are adsorption capacity of the material at any time and equilibrium, respectively, k_1 (1/min) and k_2 (CFU/mg· min) are the adsorption rate constant of Pseudo-first-order and Pseudo-second-order sorption, respectively, α is the initial adsorption rate (CFU/mg·min), and β (g/CFU) is adsorption constant, were used to describe the adsorption process. As shown in **Fig. S3**, the equilibrium data well fitted the Elovich model with a highest regression coefficient ($R^2 = 0.85$), indicating that the adsorption surface is non-uniform or energetically heterogeneous (Nizam, Krishnan, Joseph, & Krishnan, 2024).

3.4.2. Adsorption isotherms

As shown in Fig. 2B, there was no dramatic difference between BIUCFP and NIUCFP in terms of adsorption capacity at low bacterial concentrations. This could be explained by the dominance of physical adsorption during this stage. However, with the increasing concentration of the target bacteria, the adsorption rate of BIUCFP surpassed that of NIUCFP and rose rapidly. This also demonstrated the effectiveness of the imprinting cavities in BIUCFP.

The Freundlich isotherm model, $lgQ = mlgC_{free} + lga$, where Q (CFU/mg) is the adsorption capacity at equilibrium, C_{free} is the equilibrium concentration of the bacteria (CFU/mL), a is a constant in the Freundlich model, associated with adsorption capacity, and m is another constant in the Freundlich model, indicating the intensity of adsorption (Cao et al., 2024), was used to describe the adsorption process. The lgQ vs lgC_{free} plot was presented in **Fig. S4** with the regression coefficient (R^2) of 0.94, indicating multilayer adsorption on the surface of the BIUCFP.

Table 1
Comparison of different methods for detecting L. *monocytogenes*.

Methods	Limit of detection	Reference
Photoluminescence immunosensors	8.3×10^2 CFU/mL	Myndrul et al., 2024
Portable paper-based multi-biocatalyst platform	10^4 CFU/mL	Zhang, Wang, Shang, Wang, & Xu, 2022
DNA biosensor	10^2 CFU/mL	Li et al., 2021
Enzyme-linked aptasensor with rolling circle amplification assay	4.6×10^2 CFU/mL	Zhan et al., 2020
BIUCFP	72 CFU/mL	This work

3.5. Detection of the L. monocytogenes

The BIUCFP was employed for detecting various concentrations of the L. *monocytogenes*, with the outcomes depicted in Fig. 2C. Corresponding to an increase in the target bacteria concentration, the recognition efficacy of the BIUCFP was enhanced, manifesting as a reduction in fluorescence intensity. Moreover, a linear regression analysis was conducted, using bacterial concentration as the x-axis and the ratio of fluorescence intensity pre and post adsorption as the y-axis, yielding the calibration plot illustrated in Fig. 2D. The fluorescence response of the BIUCFP demonstrated a robust linear correlation across the bacterial concentration range of 10^1 to 10^7 CFU/mL. The derived linear equation was $y = 0.501x + 0.594$ ($R^2 = 0.99624$). The limit of detection (LOD) for the developed fluorescence analysis was calculated to be 72 CFU/mL by the 3σ/S rule (σ is the standard deviation of blank measurements, and S is the slope of the calibration line).

Furthermore, we conducted a comparative analysis of our methodology against other techniques documented in the literature, with the findings presented in Table 1. The comparative data reveals that the limit of detection (LOD) of our developed method is lower, indicating enhanced sensitivity. Most importantly, this imprinted upconversion fluorescence probe for L. *monocytogenes* sensing can avoid the background fluorescence interference from the sample matrixes, improving the accuracy and sensitivity of the detection method.

The specificity of the BIUCFP-based fluorescence analysis was evaluated by sensing L. *monocytogenes* (10^3 CFU/mL), *Escherichia coli* (*E. coli*, 10^5 CFU/mL), *Staphylococcus aureus* (*S. aureus*, 10^5 CFU/mL), *Bacillus subtilis* (*B. subtilis*, 10^5 CFU/mL), *Shewanella putrefaciens* (*S. putrefaciens*, 10^5 CFU/mL), and *Salmonella Enteritidis* (*S. enteritidis*, 10^5 CFU/mL). As shown in Fig. 2E, only L. *monocytogenes* gave a significantly fluorescence quenching. Little influence of the other bacteria on the fluorescence intensity are found, even at higher concentrations. Therefore, BIUCFP probe exhibited notable selectivity toward the target bacteria, which is mainly attributed to the complementary shape and size of binding sites that were produced by the template bacteria, and the electrostatic interactions between the BIUCFP and the target (Zhao et al., 2019).

RSD was used to assess the reproducibility and stability of the fluorescent material. As shown in **Table. S1**, RSD value of 15.7% for the binding capacity of BIUCFP prepared at the same condition was obtained, suggesting the reproducibility of the fluorescent probe is acceptable. The storage stability of the BIUCFP was also assessed. As shown in **Fig. S5**, the fluorescence data of the BIUCFP displayed an insignificant change within 50 days (RSD = 3.7%), revealing that the BIUCFP enjoyed good storage stability.

Table 2
Determination of L. *monocytogenes* in salmon and chicken.

Sample	Spiked (CFU/g)	Detection value (CFU/g)	Recover (%)	RSD (%)
Salmon	1.1×10^2	1.021×10^2	92.8	7.8
	4.5×10^4	4.380×10^4	97.3	10
	1.3×10^6	1.499×10^6	115.3	5.3
Chicken	1.0×10^2	0.943×10^2	97.3	3.2
	1.3×10^4	1.093×10^4	93.6	9.7
	1.1×10^6	0.963×10^6	104.8	10.0

Table 3
Detection of *L. monocytogenes* in salmon and chicken by plate counting method.

Sample	Concentration of spiked bacteria (CFU/g)	Adsorption capacity (CFU/mg)	SD
Salmon	1.8×10^1	N.D.	–
	4.0×10^1	1	0.1
	1.1×10^2	4	0.3
	1.9×10^3	91	8
	4.5×10^4	497	25
	1.3×10^6	2600	272
Chicken	1.1×10^1	N.D.	–
	5.5×10^1	2	0.1
	1.0×10^2	8	1
	2.2×10^3	109	8
	1.3×10^4	375	35
	1.1×10^6	2303	270

3.6. Real sample test

To ascertain the practical applicability of the developed method, salmon and chicken breast samples were selected for testing. As indicated in Table 2, the recovery rates of the salmon samples varied from 92.8% to 115.3%, with relative standard deviations (RSD) ranging from 5.3% to 10%. Similarly, the chicken breast samples showed recovery values ranging from 93.6% to 104.8%, with RSD values spanning 3.2% and 10%. These results indicated that the developed detection method based on the BIUCFP can be used for the quantitative analysis of L. *monocytogenes* in real-world samples.

For further assessment of the accuracy of the detection outcomes, the plate counting method, recognized as a standard method, was employed for validation. After adsorption, 1 mL of PBS buffer was added to the BIUCFP probe, shake on the shaker for a period, and bacterial colony counts were determined. As reflected in Table 3, the minimum detection level for salmon and chicken breast is 40 CFU/g and 55 CFU/g, respectively. These findings confirm that the detection results achieved using our developed method are both accurate and reliable.

4. Conclusions

In summary, a novel fluorescence probe was successfully synthesized by Pickering emulsion polymerization combining the autofluorescence-background-free trait of ACC-modified β-$NaYF_4$: Yb^{3+}, Er^{3+} upconversion nanoparticle and the specific recognition property of the imprinted polymers. A 980 nm-triggered fluorescence assay based on the BIUCFP for L. *monocytogenes* detection was developed with good selectivity, accuracy and high sensitivity. Satisfied results of the fluorescent detection method applied in salmon and chicken samples indicated that the BIUCFP synthesized in this study is reliable, with potential application in food safety monitoring and public health protection.

Consent for publication

Not applicable.

CRediT authorship contribution statement

Taotao Ren: Writing – original draft, Validation, Resources, Methodology, Investigation, Data curation. **Peng Liu:** Resources, Investigation, Formal analysis, Data curation. **Xuelian Hu:** Validation, Methodology, Investigation, Formal analysis. **Wenxiu Wang:** Visualization, Validation, Resources, Data curation. **Shuo Wang:** Validation, Resources, Formal analysis. **Xiuying Liu:** Resources, Methodology, Investigation, Formal analysis, Data curation. **Yiwei Tang:** Writing – original draft, Investigation, Formal analysis.

Declaration of competing interest

The authors declare that they have no known competing financial interests or personal relationships that could have appeared to influence the work reported in this paper.

Data availability

Data will be made available on request.

Acknowledgment

This work was financially supported by the Scientific Research Foundation for the Introduced Talent of Hebei Agricultural University (No. YJ201911).

Appendix A. Supplementary data

Supplementary data to this article can be found online at https://doi.org/10.1016/j.fochx.2024.101618.

References

Aleem, A. R., Chen, R., Wan, T., Song, W., Wu, C., Qiu, X., & Wen, H. (2024). Highly water-soluble and biocompatible hyaluronic acid functionalized upconversion nanoparticles as ratiometric nanoprobes for label-free detection of nitrofuran and doxorubicin. *Food Chemistry, 438, Article 137961*. https://doi.org/10.1016/j.foodchem.2023.137961

Al-Nayili, A., & Alhaidry, W. A. (2023). Batch to continuous photocatalytic degradation of phenol using nitrogen-rich g-C_3N_4 nanocomposites. *Research on Chemical Intermediates, 49*, 4239–4255. https://doi.org/10.1007/s11164-023-05099-z

Basak, S., Venkatram, R., & Singhal, R. S. (2022). Recent advances in the application of molecularly imprinted polymers (MIPs) in food analysis. *Food Control, 139, Article 109074*. https://doi.org/10.1016/j.foodcont.2022.109074

Bundidamorn, D., Supawasit, W., & Trevanich, S. (2021). Taqman® probe based multiplex RT-PCR for simultaneous detection of *Listeria monocytogenes*, *Salmonella spp.* and Shiga toxin-producing *Escherichia coli* in foods. *LWT, 147, Article 111696*. https://doi.org/10.1016/j.lwt.2021.111696

Cai, Y., Yang, S., Chen, D., Li, N., Xu, Q., Li, H., He, J., & Lu, J. (2017). A novel strategy to immobilize bacteria on polymer particles for efficient adsorption and biodegradation of soluble organics. *Nanoscale, 9*, 11530–11536. https://doi.org/10.1039/c7nr02610b

Cao, C., Li, Y., Fu, A., Deng, G., Li, X., Li, Y., & Qiu, X. (2024). Proposal and application of a novel isothermal model for the thermodynamic study of ion exchange reactions. *Chemical Engineering Journal, 489*, Article 151497. https://doi.org/10.1016/j.cej.2024.151497

Cardoso, A. T., Martins, R. O., Lanças, F. M., & Chaves, A. R. (2023). Molecularly imprinted polymers in online extraction liquid chromatography methods: Current advances and recent applications. *Analytica Chimica Acta, 1284*. https://doi.org/10.1016/j.aca.2023.341952. article 341952.

Chen, G., Zhang, S., Ma, X., Wilson, G., Zong, R., & Fu, Q. (2024). Antibody mimics for precise identification of proteins based on molecularly imprinted polymers: Developments and prospects. *Chemical Engineering Journal, 480, Article 148115*. https://doi.org/10.1016/j.cej.2023.148115

Dar, K. K., Shao, S., Tan, T., & Lv, Y. (2020). Molecularly imprinted polymers for the selective recognition of microorganisms. *Biotechnology Advances, 45, Article 107540*. https://doi.org/10.1016/j.biotechadv.2020.107640

Donoso, W., Castro, R. I., Guzman, L., Lopez-Cabana, Z., Nachtigall, F. M., & Santos, L. S. (2017). Fast detection of *Listeria monocytogenes* through a nanohybrid quantum dot complex. *Analytical and Bioanalytical Chemistry, 409*, 5359–5371. https://doi.org/10.1007/s00216-017-0481-9

Duze, S. T., Marimani, M., & Patel, M. (2021). Tolerance of *Listeria monocytogenes* to biocides used in food processing environments. *Food Microbiology, 97, Article 103758*. https://doi.org/10.1016/j.fm.2021.103758

Guan, T., Liu, Y., Li, J., Chen, M., Shang, X., Hu, P., & …Chen, X.. (2023). Near-infrared-triggered chirality-dependent photodynamic therapy based on hybrid upconversion nanoparticle hydrogels. *Chemical Engineering Journal, 474, Article 145429*. https://doi.org/10.1016/j.cej.2023.145429

Guk, K., Yi, S., Kim, H., Kim, S., Lim, E. K., Kang, T., & Jung, J. (2024). PoreGlow: A split green fluorescent protein-based system for rapid detection of *Listeria monocytogenes*. *Food Chemistry, 438, Article 138043*. https://doi.org/10.1016/j.foodchem.2023.138043

Hammons, S. R., Stasiewicz, M. J., Roof, S., & Oliver, H. F. (2015). Aerobic plate counts and ATP levels correlate with *Listeria monocytogenes* detection in retail delis. *Journal of Food Protection, 78*, 825–830. https://doi.org/10.4315/0362-028X.JFP-14-500

Jamieson, O., Betlem, K., Mansouri, N., Crapnell, R. D., Vieira, F. S., Hudson, A., Banks, C. E., , … Peeters, & M.. (2021). Electropolymerised molecularly imprinted polymers for the heat-transfer based detection of microorganisms: A proof-of-concept study using yeast. *Thermal Science and Engineering Progress, 24, Article 100956*. https://doi.org/10.1016/j.tsep.2021.100956

Li, Y., Chenm, M., Fan, X., Peng, J., Pan, L., Tu, K., & Chen, Y. (2022). Sandwich fluorometric method for dual-role recognition of *Listeria monocytogenes* based on antibiotic-affinity strategy and fluorescence quenching effect. *Analytica Chimica Acta, 1221*. https://doi.org/10.1016/j.aca.2022.340085. article 340085.

Li, Y., Wu, L., Wang, Z., Tu, K., Pan, L., & Chen, Y. (2021). A magnetic relaxation DNA biosensor for rapid detection of *Listeria monocytogenes* using phosphatase-mediated Mn(VII)/Mn(II) conversion. *Food Control, 125, Article 107959*. https://doi.org/10.1016/j.foodcont.2021.107959

Liu, R., Zhang, Y., Ali, S., Haruna, S. A., He, P., Li, H., … Chen, Q. (2021). Development of a fluorescence aptasensor for rapid and sensitive detection of *Listeria monocytogenes* in food. *Food Control, 122, Article 107808*. https://doi.org/10.1016/j.foodcont.2020.107808

Liu, T., Liu, X., Feng, Y., & Ya, C. J. (2023). Advances in plasmonic enhanced luminenscence of upconversion nanoparticles. Materialstoday. *Chemistry, 34, Article 101788*. https://doi.org/10.1016/j.mtchem.2023.101788

Liu, Y., Wang, L., Li, H., Zhao, L., Ma, Y., Zhang, Y., Liu, J., & Wei, Y. (2024). Rigorous recognition mode analysis of molecularly imprinted polymers-rational design, challenges, and opportunities. *Progress in Polymer Science, 150, Article 101790*. https://doi.org/10.1016/j.progpolymsci.2024.101790

Liu, Y., Zhu, H., Dou, X., Jia, K., Panagou, E. Z., Zhang, H., Xu, A., & Dong, Q. (2023). The influence of nutrients on biofilm formation of an ST87 strain of *Listeria monocytogenes*. LWT-food. *Science and Technology, 191, Article 115658*. https://doi.org/10.1016/j.foodres.2024.114010

Lopes-Luz, L., Mendonça, M., Fogaça, M. B. T., Saavedra, D. P., Bentivoglio-Silva, B. G., Conceição, F. R., & Bührer-Sékula, S. (2023). Detection of *Listeria monocytogenes* using an immunochromatographic point of care test based on anti-internalin a and B antibodies and a nano-biotinylated detection complex. *LWT, 188, Article 115336*. https://doi.org/10.1016/j.lwt.2023.115336

Magalhães, R., Mena, C., Ferreira, V., Almeida, G., Silva, J., & Teixeira, P. (2021). Traditional methods of analysis for *Listeria monocytogenes*. In E. M. Fox, H. Bierne, & B. Stessl (Eds.), *Vol. 2220. Listeria Monocytogenes. Methods in molecular biology*. https://doi.org/10.1007/978-1-0716-0982-8_1. Humana, New York, NY.

Mahata, M. K., & Lee, K. T. (2019). Development of near-infrared sensitized core-shell-shell upconverting nanoparticles as pH-responsive probes. *Nanoscale Advances, 1*, 2372–23781. https://doi.org/10.1039/c9na00088g

Myndrul, V., Yanovska, A., Babayevska, N., Korniienko, V., Diedkova, K., Jancelewicz, M., Pogorielov, M., & Iatsunskyi, I. (2024). 1D ZnO-au nanocomposites as label-free photoluminescence immunosensors for rapid detection of *Listeria monocytogenes*. *Talanta, 271*, Article 125641. https://doi.org/10.1016/j.talanta.2024.125641

Nizam, T., Krishnan, K. A., Joseph, A., & Krishnan, R. R. (2024). *Isotherm, kinetic and thermodynamic modelling of liquid phase adsorption of the heavy metal ions Zn(II), Pb(II) and Cr(VI) onto $MgFe_2O_4$ nanoparticles. Groundwater for sustainable development, 25, article 101120*. https://doi.org/10.1016/j.gsd.2024.101120

Pan, T., Chen, H., Gao, X., Wu, Z., Ye, Y., & Shen, Y. (2022). Engineering efficient artificial nanozyme based on chitosan grafted Fe-doped-carbon dots for bacteria biofilm eradication. *Journal of Hazardous Materials, 435, Article 128996*. https://doi.org/10.1016/j.jhazmat.2022.128996

Prasad, M. C. B., Milton, A. A. P., Menon, V. K., Srinivas, K., Bhargavi, D., Das, S., & Thomas, N. (2024). Development of a novel visual assay for ultrasensitive detection of *Listeria monocytogenes* in milk and chicken meat harnessing helix loop-mediated isothermal amplification (HAMP). *Food Control, 155, Article 110081*. https://doi.org/10.1016/j.foodcont.2023.110081

Ren, L., Hong, F., Feng, N., Lin, J., Wang, J., Ruan, S., & Chen, Y. (2024). An eco-friendly and ultrasensitive micro-orifice resistance assay for the detection of *Listeria monocytogenes* based on calcium carbonate signal probes harvested from discarded eggshells. *Sensors and Actuators B: Chemical, 405, Article 135312*. https://doi.org/10.1016/j.snb.2024.135312

Roumani, F., Azinheiro, S., Carvalho, J., Prado, M., & Garrido-Maestu, A. (2021). Loop-mediated isothermal amplification combined with immunomagnetic separation and propidium monoazide for the specific detection of viable *Listeria monocytogenes* in milk products, with an internal amplification control. *Food Control, 125, Article, 107975*. https://doi.org/10.1016/j.foodcont.2021.107975

Salman, N. S., & Alshamsi, H. A. (2022). Synthesis of sulfonated polystyrene-based porous activated carbon for organic dyes removal from aqueous solutions. *Journal of Polymers and the Environment, 30*, 5100–5118. https://doi.org/10.1007/s10924-022-02584-1

Silva, N. F. D., Neves, M. M. P. S., Magalhães, J. M. C. S., Freire, C., & Delerue-Matos, C. (2020). Emerging electrochemical biosensing approaches for detection of *Listeria monocytogenes* in food samples: An overview. *Trends in Food Science & Technology, 99*, 621–633. https://doi.org/10.1016/j.tifs.2020.03.031

Tominaga, T. (2017). Enhanced sensitivity of lateral-flow test strip immunoassays using colloidal palladium nanoparticles and horseradish peroxidase. *LWT, 86*, 566–570. https://doi.org/10.1016/j.lwt.2017.08.027

Xiao, F., Wang, Z., Li, W., Qi, W., Bai, X., & Xu, H. (2023). Cefepime-modified magnetic nanoparticles and enzymatic colorimetry for the detection of *Listeria monocytogenes* in lettuces. *Food Chemistry, 409, Article 135296*. https://doi.org/10.1016/j.foodchem.2022.135296

Zakrzewski, A. J., Gajewska, J., Chajęcka-Wierzchowska, W., Załuski, D., & Zadernowska, A. (2023). Prevalence of *Listeria monocytogenes* and other Listeria species in fish, fish products and fish processing environment: A systematic review and meta-analysis. *Science of the Total Environment, 907, Article 167912*. https://doi.org/10.1016/j.scitotenv.2023.167912

Zhan, Z., Li, H., Liu, J., Xie, G., Xiao, F., Wu, X., … Xu, H. (2020). A competitive enzyme linked aptasensor with rolling circle amplification (ELARCA) assay for colorimetric detection of *Listeria monocytogenes*. *Food Control, 107, Article 106806*. https://doi.org/10.1016/j.foodcont.2019.106806

Zhang, J., Wang, Y., & Lu, X. (2021). Molecular imprinting technology for sensing foodborne pathogenic bacteria. *Analytical and Bioanalytical Chemistry, 413*, 4581–4598. https://doi.org/10.1007/s00216-020-03138-x

Zhang, Y., Wang, H., Shang, K., Wang, X., & Xu, P. (2022). Reliable detection of *Listeria monocytogenes* by a portable paper-based multi-biocatalyst platform integrating three biomarkers: Gene hly, acetoin, and listeriolysin O protein. *Journal of Electroanalytical Chemistry, 905, Article 115975*. https://doi.org/10.1016/j.jelechem.2021.115975

Zhao, X., Cui, Y., Wang, J., & Wang, J. (2019). Preparation of fluorescent molecularly imprinted polymers via Pickering emulsion interfaces and the application for visual sensing analysis of *Listeria monocytogenes*. *Polymers (Basel), 11*, 1–13. https://doi.org/10.3390/polym11060984